Optics Communications 465 (2020) 125620

Contents lists available at ScienceDirect

Optics Communications

journal homepage: www.elsevier.com/locate/optcom

High-performance 90° hybrids based on MMI couplers in Si_3N_4 technology

Jia Yu [a,1], Jinfeng Mu [b,1], Kaixuan Chen [a], Michiel de Goede [b], Meindert Dijkstra [b], Sailing He [a,*], Sonia M. García-Blanco [b]

[a] Centre for Optical and Electromagnetic Research, College of Optical Science and Engineering, State Key Laboratory of Modern Optical Instrumentation Zhejiang University, Hangzhou, 310027, China

[b] Optical Sciences Group, MESA+ Institute for Nanotechnology, University of Twente, P.O. Box 217, 7500 AE, Enschede, The Netherlands

ARTICLE INFO

Keywords:
Integrated optics
Silicon nitride (Si_3N_4)
Optical 90° hybrid
Multimode interference (MMI) coupler

ABSTRACT

Low-loss, broadband, and low phase deviation optical 90° hybrids based on 2 × 4 multimode interference couplers are firstly demonstrated using Si_3N_4 on SiO_2 technology. Only a simple traditional design method of MMI based on self-imaging theory and a single-stripe Si_3N_4 waveguide geometry with only one step etching process are utilized. The characterization of the fabricated devices is carried out over a wide spectral window of 1520–1610 nm, showing that the measured phase error is less than 8°, and common-mode rejection ratios (CMRRs) are better than −20 dB. The measured total loss of the fabricated device including a 90° hybrid and a 3-dB coupler is <1 dB in a bandwidth over 80 nm. Our analysis also shows large fabrication tolerance with width of ±0.1 μm or length of ±3 μm.

1. Introduction

Optical 90° hybrids permit maximizing spectral efficiency and receiver sensitivity in higher-order modulation schemes, such as quadrature phase shift keying (QPSK) in coherent detection systems [1]. Low loss, low phase error, high common-mode rejection ratio (CMRR), and broadband operation are required to demodulate the optical signal accurately. Previously, multimode interference (MMI) couplers have been employed to realize high-performance hybrids on several photonic technologies such as the InP [2] and the silicon-on-insulator (SOI) platforms [3]. In these high refractive index contrast platforms, methods based on the optimization of the index-contrast are normally used to avoid the strong phase errors introduced by the high-order modes in the MMI hybrids. Such methods include shallow etched waveguides [4] and subwavelength gratings in the lateral cladding of the MMI region [5]. However, these methods require high-resolution lithography tools and precise control of the dry etching process, resulting in reduced tolerance for dimensional deviation during fabrication. In other approaches, such as using a wedge-shaped MMI hybrid [6] to reduce the mode number in order to eliminate the strong phase error of the high-order modes, the bandwidth is limited. Besides these high refractive index contrast platforms, 90° hybrids in relatively low refractive index contrast polymer (SU-8) platform have shown low-loss and good performance for polarization demultiplexing [7] but the bandwidth and durability of the devices is limited due to the polymer properties.

Silicon nitride (Si_3N_4) has been widely employed recently in *nonlinear optics* [8], bio-sensing [9] and *microwave photonics* [10] owing to its low propagation loss (<0.1 dB/cm), and large transparency window (400–2350 nm) [11]. Compared to the aforementioned technologies, the Si_3N_4 platform shows a great potential for the realization of low-loss, low phase error, and broadband 90° hybrids based on MMIs due to its moderate index contrast and low propagation loss [12]. In this paper, an optical 90° hybrid on a single-stripe Si_3N_4 platform is presented. The dimensional parameters are first extracted by a 2D mode simulation and further investigated using a 3D finite time different domain (FDTD) method. The Si_3N_4 waveguides are fabricated by a full dry etching process and cladded by SiO_2. The fabricated chips are characterized in a spectral window of 1520–1610 nm. The measured result with optimal design at the MMI length of 270 μm shows losses of below 1 dB for wavelength band larger than 80 nm. The measured phase deviation between the output ports are below 6° in the C-band and within 8° for the whole measured spectral range. CMRRs better than −20 dBe have also been demonstrated.

2. Device design

Fig. 1 shows the schematic of the 90° hybrid based on an MMI, where a 200 nm thick Si_3N_4 on an 8 μm thick thermal oxide is employed. The device is designed to work under transverse-electric (TE) polarization. The 90° phase relations of the output locations of the MMI are in accordance with the self-imaging theory [13,14]. To ensure high

* Corresponding author.
E-mail address: sailing@zju.edu.cn (S. He).
[1] J. Yu and J. Mu are co-first authors.

https://doi.org/10.1016/j.optcom.2020.125620
Received 23 January 2020; Received in revised form 25 February 2020; Accepted 25 February 2020
Available online 27 February 2020

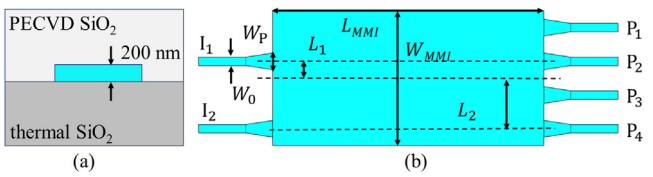

Fig. 1. Schematic of the 90° hybrid: (a) cross-section of the 200 nm thick Si_3N_4 waveguide, and (b) the top-view layout of the device.

quality imaging, the 2 × 4 MMI has to demonstrate low phase errors for the modes, especially the higher-order modes. *Additionally, adequate space between the input/output ports is required to reduce the mutual cross-talk. Thus, the MMI width should not be too small. Although a larger MMI width may lead to lower loss and lower phase errors of the device, it results in larger dimensions. With an overall balanced consideration for the loss, phase error and size, we choose the MMI width as* $W_{MMI} = 16$ μm, *at which the MMI supports 10 TE modes.*

The 2D mode simulations are carried out using the commercial suite Optodesigner (Phoenix B.V.). The refractive indices of Si_3N_4 and SiO_2 utilized are 1.984 and 1.446 respectively at 1550 nm. The calculated phase error of the highest order (10th) mode, i.e., the difference between the simulated phase change after fourfold imaging distance propagation and the ideal parabolic phase relations of different modes shown in [13], is ~48°, which is comparable to the phase error obtained in SOI (i.e., ~58°) by the shallow etching technique [4], indicating that the 200 nm thick Si_3N_4 platform intrinsically has lower phase errors. In Fig. 1, the distances of the input port I_1 and output ports P_2 and P_3 to the center of the MMI are chosen to be 2 μm and labeled L_1. Meanwhile, other distances between the input port I_2 and the output ports P_1 and P_4 to the center of MMI are selected to be 6 μm and denoted as L_2. The widths of the input/output ports are optimized to $W_p = 3$ μm, following the approach presented in the work of [14] and are linearly tapered to $W_0 = 1.2$ μm using adiabatic tapers with a length of 15 μm, which avoids the excitation of unwanted higher-order modes. With these parameters, the cross-talks are found to be negligible at the output ports due to sufficient separation distance (i.e., 4 μm).

The performance of the device based on the full 3D structure is calculated using 3D FDTD over a wide spectral range of 1520–1580 nm. For simplicity, the aforementioned refractive indices at a wavelength of 1550 nm are employed in the simulation.

Firstly, an MMI width of 16 μm is studied in 3D FDTD. The MMI length (L_{MMI}) is chosen to be 270 μm, which is equal to three-quarters of the beat length at the wavelength of 1550 nm ($3L_\pi/4$). At this length, the excess losses of the hybrid, as shown in Fig. 2(a), are 0.13 dB at 1550 nm and below 0.21 dB for the entire C-band (i.e., 1530–1565 nm). The loss gradually rises as the wavelength increases over 1550 nm. This is because the MMI length is no longer optimal due to the variation of the corresponding effective refractive indices of the modes in the MMI region caused by the wavelength change.

The hybrid phase deviations of the output ports referring to the output port 3 are calculated as $\Delta\phi_{13} = \phi_1 - \phi_3 - 90°$, $\Delta\phi_{23} = \phi_2 - \phi_3 - 180°$ and $\Delta\phi_{34} = \phi_3 - \phi_4 - 90°$, where $\phi_{i,j}$ is the phase of the output port i or j, and $i, j = 1, 2, 3, 4$ indicate different output ports. It can be seen from Fig. 2(b) that all the phase deviations are within 5° in the investigated spectral range for the hybrid, indicating strong broadband properties of the hybrid.

Additionally, *the common mode rejection ratios (CMRR) quantitatively imply the relative weakness of the power detected by a pair of balanced photo-detectors* [15]. Both CMRRs between in-phase channels (I), i.e., P_1 and P_4, and quadrature channels (Q), i.e., P_2 and P_3, are calculated as $20\log[(P_i - P_j)/(P_i + P_j)]$, where $P_{i,j}$ is the power of the output port i or j. Fig. 2(c) and (d) show the calculated values of CMRRs for the input ports 1 and 2, respectively. The CMRRs are better than −20 dB, resulting in a good power balance between both in-phase and quadratic channels, meaning the hybrid is qualified for operation as a coherent optical receiver. *Additionally, it can be seen that there are some dips in the CMRR curves. The power of the corresponding two output ports are equal at the wavelength of dip position, and thus the corresponding CMRR drops to zero according to its definition.*

The influence of the variation of dimensional parameters of the MMI on the hybrid performance are studied. In particular, the width variation originating from the fabrication deviation using standard lithography (<0.2 μm) leads to changes in the effective refractive indices of the modes in the MMI, which significantly affects the phases of

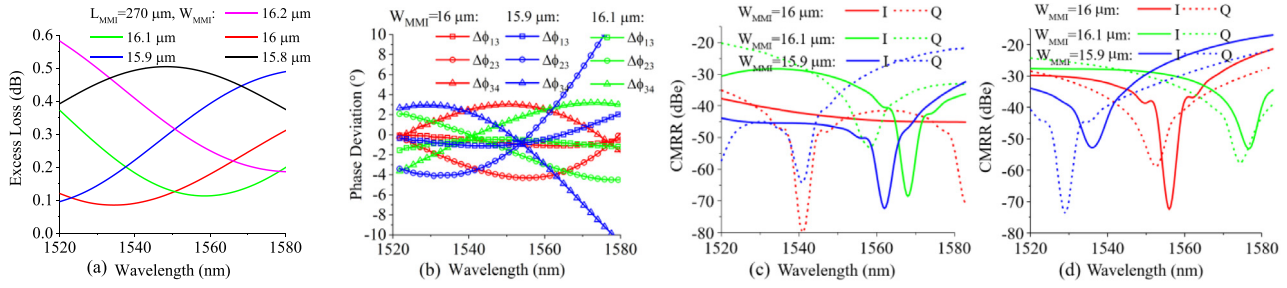

Fig. 2. Parameters of the hybrid at different MMI widths with a fixed MMI length of 270 μm: (a) calculated hybrid loss, (b) the phase deviations between different output ports, (c) the CMRRs of in-phase and quadrature channels with input port 1, and (d) the CMRRs with input port 2.

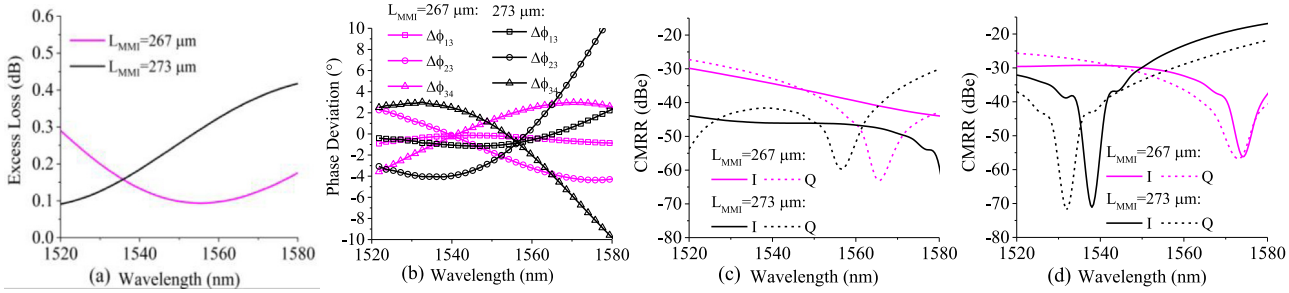

Fig. 3. Parameters of the hybrid at different MMI lengths with a fixed MMI width of 16 μm: (a) Calculated hybrid loss, (b) the phase deviations between different output ports, (c) the CMRRs of in-phase and quadrature channels with input port 1, and (d) the CMRRs with input port 2.

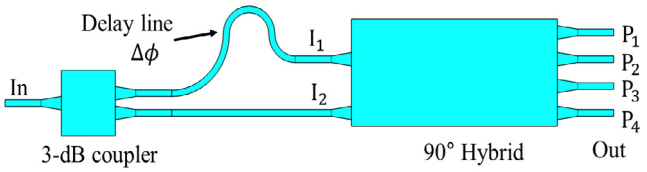

Fig. 4. Schematic of the 3-dB coupler integrated hybrid.

the modes at the output ports after propagation as well as their imaging patterns. Fig. 2(a) also shows the losses considering a variation of the width of the MMI from 15.8 μm to 16.2 μm. With the increase of the deviation from the nominal 16 μm, the loss curve in the C-band rises, indicating that the hybrid is sensitive to the MMI width and a precise control of the width is required during the lithography step. Hence, for the phase deviation and CMRR, an MMI with widths of 15.9 μm and 16.1 μm at a length of 270 μm, where the minimum of the loss shifts to wavelengths of 1520 nm and 1560 nm, respectively, is considered for the width tolerance study, as shown in Fig. 2(b)–(d). The phase deviation $\Delta\phi_{13}$ remains stable with the variation of the MMI width. The deviations $\Delta\phi_{23}$ and $\Delta\phi_{34}$ at the width of 16.1 μm still remain within 5°. However, they rise considerably after a wavelength of 1560 nm at a width of 15.9 μm. The CMRRs for both in-phase and quadrature channels at the width of 16.1 μm are still better than −20 dB, while one of the in-phase channels with input port 2 fails for an MMI width of 15.9 μm.

The beat length change is found to be about 4.5 μm for a 0.1 μm variation of the MMI width, according to 2D mode solver calculations, which requires the length of MMI hybrid to be varied about 3.4 μm (i.e., three-quarters of beat length) in the design in order to compensate for width variation. Therefore, the parameters of the hybrids with the MMI length of 267 μm and 273 μm for the nominal MMI width of 16 μm are simulated by 3D FDTD, and are shown in Fig. 3(a)–(d). As expected, for MMI lengths of 267 μm and 273 μm, the tendencies of the loss and phase deviations as a function of wavelength are similar to those of MMIs of widths 16.1 μm and 15.9 μm [Figs. 2(a) and 2(b)], respectively and nominal length of 270 μm. Except for the in-phase channel CMRR at the length of 273 μm with input port 2, CMRRs better than −20 dBe over the investigated spectral window have been simulated. *For a thickness tolerance of* ±2 nm*, which can be achieved by the state-of-the-art deposition technology, the influence of the thickness variation to the simulated performance is very small, which can be negligible.*

3. Experiment results

A single-stripe layer of Si_3N_4 was deposited by low pressure chemical vapor deposition (LPCVD) on thermally oxidized silicon wafers with 8 μm thick silicon dioxide. The fabrication of the Si_3N_4 waveguides follows the process flow presented in [16] by using standard optical lithography (EVG620) and plasma etching (Adixen AMS100). After fabricating the waveguides, a layer of SiO_2 with ~6 μm thick was deposited on top of the device by plasma enhanced chemical vapor deposition (PECVD) to serve as top cladding.

In the fabricated chip, a 3-dB power splitting coupler is integrated for testing purposes, as shown in Fig. 4. The coupler has a width of 5 μm and a length of 15 μm, which is equal to $3L_\pi/8$. Its input and output ports are linearly tapered from 2 μm to 1.2 μm with a taper length of 15 μm. Its excess loss is calculated to be 0.2 dB. The purpose of using this coupler is to form a Mach–Zehnder interferometer (MZI) with the hybrid, where the arm connected to input port 1 has an additional length that introduces a phase delay of $\Delta\phi$ with respect to the arm connected to input port 2. Therefore, a wavelength-dependent phase shift can be obtained between the hybrid input ports, which allows for extraction of the phase deviations between the output ports through characteristic filter transmission curves by directly scanning the wavelength.

In the characterization setup, a laser tunable from 1520 nm to 1610 nm (Agilent 81940A) is used. Single-mode fibers with a mode size of ~10 μm and inverse tapers on Si_3N_4 chip are employed for the light input and output. The transmission spectrum of each output port is measured for the full spectral window. A neighboring straight waveguide with the same width (2 μm) is used as a reference waveguide. Fig. 5(a) shows the measured spectra of the 90° hybrid with the MMI length of 270 μm in the range of, as an example, 1545–1555 nm. The high extinction ratios (>20 dB) are due to the perfect imaging in Si_3N_4 hybrid and the uniform power splitting ratio (50 ± 3: 50 ± 3 over the measured spectral range) in 3-dB coupler.

The total loss, which includes the loss of the hybrid and the loss of the 3-dB coupler, is extracted by subtracting the maximum values of the measured spectrum to the one of the reference straight waveguide, where the effect of the coupling losses and most of the Si_3N_4 propagation losses are eliminated. Moreover, the influence of the propagation losses of the Si_3N_4 waveguide is neglected due to its low loss (measured to be ~0.14 dB/cm at 1550 nm). Fig. 5(b) shows the extracted total losses for the MMI lengths of 270 μm and 273 μm. Due to a defect at one of the output ports on the fabricated chip, the results of the hybrid at an MMI length of 267 μm are not shown here. It can be seen that the total loss (i.e., 90° hybrid and 3 dB coupler) at the MMI length of 270 μm is below 1 dB over an 80 nm bandwidth.

The peaks/valleys in each measured spectrum of Fig. 5(a) are separated by the free spectral range (FSR) due to the delay line of the MZI. Each period represents a 2π phase shift. The wavelength separation ($\Delta\lambda$) between the minima of the spectra of output ports i and j relates to the phase deviation $\Delta\phi_{i,j}$, which can be expressed as $\Delta\phi_{i,j} = 2\pi\Delta\lambda/\mathrm{FSR}$ (Fig. 6). In the spectral window considered in this work, the phase deviations of the output ports or an MMI 270 μm long are all found within 6° in the C-band and within 8° over an 80 nm bandwidth. Additionally, the hybrid with an MMI length of 273 μm has a higher phase deviation. An increasing trend can be found when the wavelength is larger than 1570 nm. The CMRRs of in-phase and quadratic channels of the fabricated device are also obtained from the measured peaks of

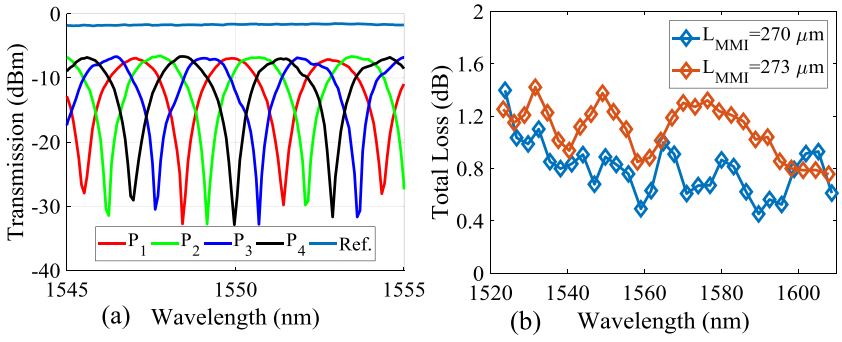

Fig. 5. (a) Measured transmission spectra of the MMI hybrid and reference waveguide. (b) The total loss of the 3-dB coupler integrated MMI hybrid.

Table 1
A comparison of 90° Hybrids.

	Total loss/dB	Phase deviation/°	CMRR/ dBe	BW/ nm	MMI Size/μm²	Technology	Fabrication tolerance
[2]	<1	<5	<−20	94	12 × 360	GaInAsP/InP, 2 × 4 MMI + Phase Shifter + 2 × 2 MMI	–
[4]	–	<5	<−20	50	7.7 × 115.5	SOI, shallowly etched MMI	–
[5]	–	<10	<−20	60	10 × 186.5	SOI, MMI with subwavelength structures	–
[6]	<1	<5	<−20	40	12 × 107	SOI, wedge-shaped MMI	–
This work	<1	<8	<−20	80	16 × 270	Si_3N_4, traditional simple MMI	±0.1 μm in width

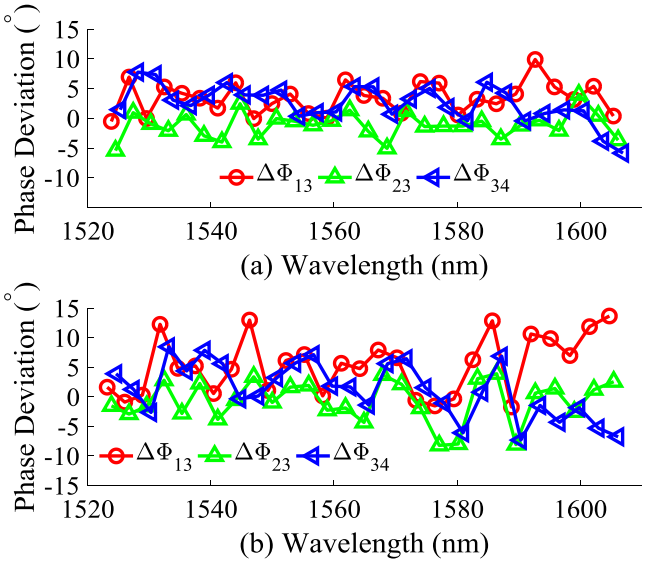

Fig. 6. The phase deviations between the output ports referring to the output port 3 at the MMI length of 270 μm (a) and 273 μm (b).

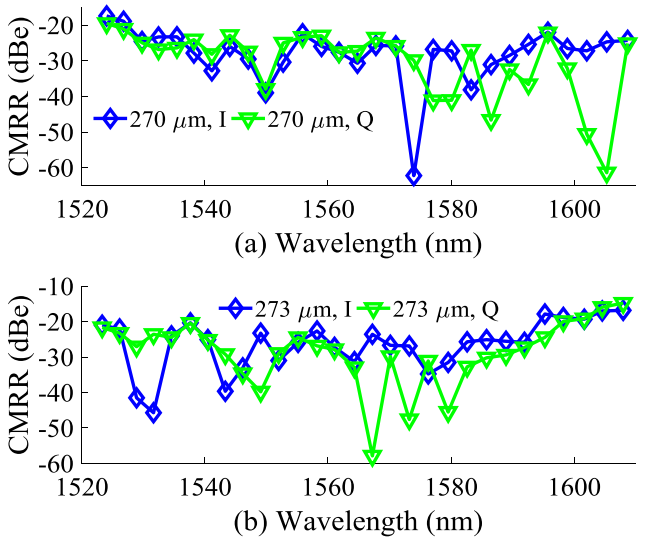

Fig. 7. The CMRRs of the 3-dB coupler integrated MMI hybrid at the MMI length of 270 μm (a) and 273 μm (b).

the spectra by calculating using aforementioned formula in the design part. In Fig. 7, the CMRRs of the hybrids at both MMI lengths are shown. For the hybrid with the nominal length of 270 μm, CMRRs better than −20 dBe can be seen in a wavelength range of 1525–1610 nm, indicating broadband operation with good power balance between the output channels. Also, less than −20 dBe CMRRs are also achieved for the hybrid with an MMI length of 273 μm in the range of 1520–1600 nm. *We compare our results with other typical works published before, as shown in Table 1. Our work has the advantages of e.g. simple design, only simple etching process required, and large fabrication tolerance while maintaining high performance. The bandwidth is much better than those of the other works except [2], where a more complicated and longer structure consisting of 2 cascaded MMI structures and a phase shifter was used.*

4. Conclusion

Optical 90° hybrids in Si_3N_4 technology have been proposed and demonstrated on a 200 nm thick single-stripe layer of Si_3N_4. The hybrids have been designed using an approach that combines a 2D mode solver and 3D FDTD simulations. The influence of the variation of the hybrid dimensional parameters on the device performance has been analyzed. The designed hybrids exhibit excellent performance. The fabricated devices have been integrated on chip with 3-dB couplers and experimentally demonstrated in a spectral window of 1520–1610 nm, showing less than 1 dB total losses, within 8° phase errors between the output ports, and better than −20 dBe common mode rejection ratios over an 80 nm bandwidth.

Declaration of competing interest

The authors declare that they have no known competing financial interests or personal relationships that could have appeared to influence the work reported in this paper.

CRediT authorship contribution statement

Jia Yu: Validation, Formal analysis, Investigation, Writing - original draft. **Jinfeng Mu:** Methodology, Validation, Data curation, Writing - original draft. **Kaixuan Chen:** Methodology, Project administration, Writing - review & editing. **Michiel de Goede:** Validation. **Meindert Dijkstra:** Validation. **Sailing He:** Conceptualization, Supervision, Funding acquisition, Writing - review & editing. **Sonia M. García-Blanco:** Supervision, Funding acquisition, Writing - review & editing.

Acknowledgments

This work was supported by the Stitching voor de Technisch Wetenschappen, The Netherlands under Project STW-13536, and the National Natural Science Foundation of China (No. 11621101) and the Fundamental Research Funds for the Central Universities, China (2017FZA5001).

References

[1] M. Seimetz, C.M. Weinert, Options, feasibility, and availability of 2×4 90° hybrids for coherent optical systems, J. Lightwave Technol. 24 (2006) 1317–1322.

[2] S.-H. Jeong, K. Morito, Novel optical 90° hybrid consisting of a paired interference based 2×4 MMI coupler, a phase shifter and a 2×2 MMI coupler, J. Lightwave Technol. 28 (2010) 1323–1331.

[3] K. Voigt, L. Zimmermann, G. Winzer, H. Tian, B. Tillack, K. Petermann, C-band optical 90° hybrids in silicon nanowaveguide technology, IEEE Photonics Technol. Lett. 23 (2011) 1769–1771.

[4] R. Halir, G. Roelkens, A. Ortega-Moñux, J. Wangüemert-Pérez, High-performance 90 hybrid based on a silicon-on-insulator multimode interference coupler, Opt. Lett. 36 (2011) 178–180.

[5] A. Ortega-Monux, L. Zavargo-Peche, A. Maese-Novo, I. Molina-Fernández, R. Halir, J. Wanguemert-Perez, P. Cheben, J. Schmid, High-performance multimode interference coupler in silicon waveguides with subwavelength structures, IEEE Photonics Technol. Lett. 23 (2011) 1406–1408.

[6] W. Yang, M. Yin, Y. Li, X. Wang, Z. Wang, Ultra-compact optical 90° hybrid based on a wedge-shaped 2×4 MMI coupler and a 2×2 MMI coupler in silicon-on-insulator, Opt. Express 21 (2013) 28423–28431.

[7] Y. Jiao, Y. Zhu, X. Hong, Y. Shi, L. Xu, S. He, An integrated optical mixer based on SU8 polymer for PDM-QPSK demodulation, IEEE Photonics Technol. Lett. 23 (2011) 1490–1492.

[8] M.A. Porcel, F. Schepers, J.P. Epping, T. Hellwig, M. Hoekman, R.G. Heideman, P.J. van der Slot, C.J. Lee, R. Schmidt, R. Bratschitsch, Two-octave spanning supercontinuum generation in stoichiometric silicon nitride waveguides pumped at telecom wavelengths, Opt. Express 25 (2017) 1542–1554.

[9] L. Gounaridis, P. Groumas, E. Schreuder, G. Tsekenis, A. Marousis, R. Heideman, H. Avramopoulos, C. Kouloumentas, High performance refractive index sensor based on low Q-factor ring resonators and FFT processing of wavelength scanning data, Opt. Express 25 (2017) 7483–7495.

[10] C.G. Roeloffzen, L. Zhuang, C. Taddei, A. Leinse, R.G. Heideman, P.W. van Dijk, R.M. Oldenbeuving, D.A. Marpaung, M. Burla, K.-J. Boller, Silicon nitride microwave photonic circuits, Opt. Express 21 (2013) 22937–22961.

[11] C.G. Roeloffzen, M. Hoekman, E.J. Klein, L.S. Wevers, R.B. Timens, D. Marchenko, D. Geskus, R. Dekker, A. Alippi, R. Grootjans, Low-loss Si_3N_4 TriPleX optical waveguides: Technology and applications overview, IEEE J. Sel. Top. Quantum Electron. 24 (2018) 1–21.

[12] L.B. Soldano, E.C. Pennings, Optical multi-mode interference devices based on self-imaging: principles and applications, J. Lightwave Technol. 13 (1995) 615–627.

[13] M. Bachmann, P.A. Besse, H. Melchior, General self-imaging properties in N × N multimode interference couplers including phase relations, Appl. Opt. 33 (1994) 3905–3911.

[14] J. Mu, S.A. Vázquez-Córdova, M.A. Sefunc, Y.-S. Yong, S.M. García-Blanco, A low-loss and broadband MMI-based multi/demultiplexer in Si_3N_4/SiO_2 technology, J. Lightwave Technol. 34 (2016) 3603–3609.

[15] Y. Painchaud, M. Poulin, M. Morin, M. Têtu, Performance of balanced detection in a coherent receiver, Opt. Express 17 (2009) 3659–3672.

[16] J. Mu, M. Dijkstra, Y.-S. Yong, F.B. Segerink, K. Wörhoff, M. Hoekman, A. Leinse, S.M. García-Blanco, Low-loss, broadband and high fabrication tolerant vertically tapered optical couplers for monolithic integration of Si_3N_4 and polymer waveguides, Opt. Lett. 42 (2017) 3812–3815.